Geophys. J. Int. (2004) **157,** 265–282 doi: 10.1111/j.1365-2966.2004.02179.x

Active faulting and seismicity of the Dasht-e-Bayaz region, eastern Iran

Richard Walker, James Jackson and Calum Baker

Bullard Laboratories, Madingley Road, Cambridge CB3 0EZ, *UK. E-mails: rwalker@esc.cam.ac.uk; jackson@esc.cam.ac.uk*

Accepted 2003 November 3. Received 2003 October 29; in original form 2002 December 10

SUMMARY

The Dasht-e-Bayaz left-lateral strike-slip fault system in NE Iran ruptured over a length of *ca* 120 km during two earthquakes in 1968 and 1979. We constrain source parameters of the 1968 August 31 (Dasht-e-Bayaz) and 1979 November 27 (Khuli-Buniabad) earthquakes by analysing long-period body wave seismograms. Both earthquakes involved complex rupture processes, with at least two subevents in each case. Coseismic surface ruptures and cumulative scarps in alluvium indicate fault segmentation on numerous short (*ca* 20 km long) strands with small pull-aparts between them. The earthquake subevents seen in the seismograms probably relate to this segmentation. The total, cumulative, offset on the fault system is estimated at *ca* 4–5 km. This is small compared to the total amount of Late Tertiary deformation expected in this part of Iran, and indicates that the Dasht-e-Bayaz fault may be relatively young. Distributed strike-slip faulting is widespread in the region and there are indications that the Dasht-e-Bayaz fault is evolving from several short faults that are coalescing. These results are important not only for understanding of the regional tectonics but for the development and evolution of strike-slip faults in general.

Key words: continental deformation, earthquakes, strike-slip faulting, Iran.

1 INTRODUCTION

Strike-slip faults over 100 km in length are seen in many regions of active continental tectonics (e.g. Molnar & Tapponnier 1975; Molnar & Deng 1984; Jackson & McKenzie 1984). These faults are capable of producing large earthquakes (Kurushin *et al.* 1997; Lasserre *et al.* 1999) and are important elements in the deformation of the continents. Intra-plate strike-slip faults do not always link with other major structures at their ends and sometimes involve rotations about vertical axes (Bayasgalan *et al.* 1999; Berberian *et al.* 2000; England & Molnar 1990). However, we know little about how such faults grow and evolve with time.

In this paper, we investigate the development of active faulting around the Dasht-e-Bayaz fault in Khorassan province, eastern Iran (Fig. 1). Abundant seismicity is recorded in this region both historically (Ambraseys & Melville 1982; Berberian & Yeats 1999) and instrumentally (Ambraseys & Tchalenko 1969; Haghipour & Amidi 1980; Berberian & Yeats 1999; Berberian *et al.* 1999) and many of these earthquakes have been assigned to particular faults (Fig. 2 and Tables 1 and 2). However, active faulting changes the topography and drainage patterns on the surface, and the geomorphology is able to retain information about fault evolution over relatively long timescales for both dip-slip (e.g. Jackson *et al.* 1996; Keller *et al.* 1998) and strike-slip (e.g. Replumaz *et al.* 2001; Talebian 2002; Walker & Jackson 2002) faults. We exploit this potential by using LANDSAT TM+ and ASTER satellite imagery to observe the effects of active faulting on the geomorphology of the Dasht-e-Bayaz region. We also use *P* and *SH* body wave inversion to constrain the source parameters of the 1968 August 31 and 1979 November 27 earthquakes on the Dasht-e-Bayaz system. Combining seismic and geomorphic data sets gives us better insight into the structure and evolution of the Dasht-e-Bayaz and surrounding faults and their importance to the local tectonics, and is relevant for our understanding of the development of intracontinental strike-slip faults in general. One of our conclusions is that the Dasht-e-Bayaz fault is unable to account for the total Late Tertiary deformation that is expected in this part of Iran and therefore that the faulting must have changed with time.

2 ACTIVE TECTONICS OF EASTERN IRAN

The active deformation of Iran accommodates Arabian–Eurasian convergence. Shortening is mainly achieved by distributed faulting in high mountain ranges in the south (the Zagros) and the north (the Alborz and Kopeh Dagh) of the country (Fig. 1a). Surrounding regions to the north and east are aseismic and appear not to be deforming (Figs 1a and b). Total Arabia–Eurasia convergence is between 28 and 40 mm yr^{-1} at 60°E. This large uncertainty is due to ambiguities in the interpretation of seafloor spreading data in the Red Sea and Gulf of Aden (DeMets *et al.* 1994; Jestin *et al.* 1994; Chu & Gordon 1998), and because of the poorly determined motion of Arabia with current GPS coverage, which gives lower estimates of

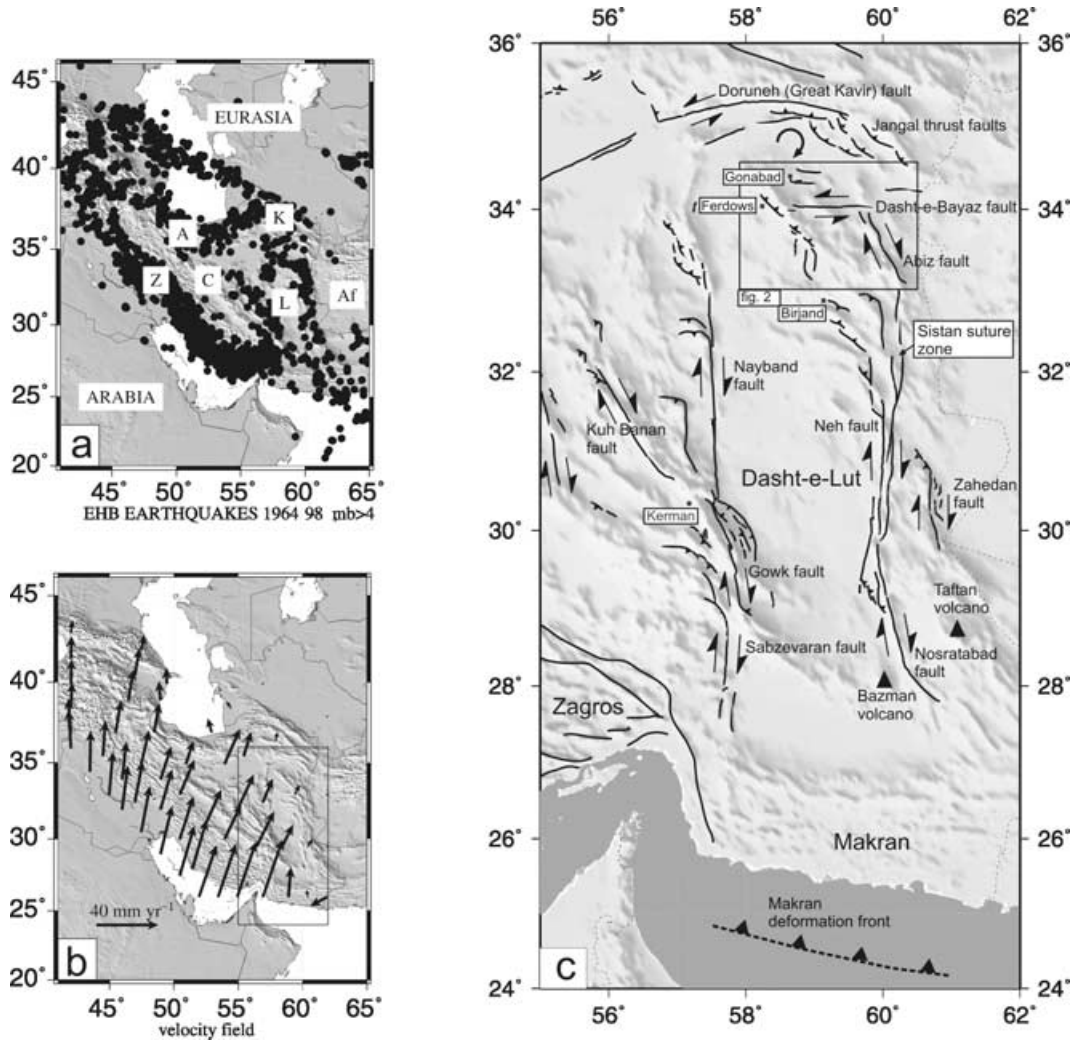

Figure 1. (a) Seismicity of Iran for the period 1964–1990. Epicentres are from Engdahl *et al.* (1998). The seismicity is mainly confined within the political borders of Iran with Eurasia and Afghanistan (Af) being essentially aseismic. Earthquake deformation within Iran is concentrated in the Zagros (Z), the Alborz (A), the Kopet Dag (K) and in eastern Iran. The aseismic central Iran and Lut blocks are denoted by C and L. (b) A velocity field for Iran estimated from the spatial variation in the style of strain rates indicated by earthquakes (from Jackson *et al.* (1995). Velocities are shown relative to stable Eurasia. The overall Arabia–Eurasia convergence is assumed to be close to that of NUVEL 1A (DeMets *et al.* 1994) and may be too high (Sella *et al.* 2002). Note the right-lateral shear expected along the eastern border of Iran. The boxed region shows the location of Fig 1(c). (c) Major faulting in eastern Iran. South of 34°N deformation occurs in two zones of N–S dextral strike-slip, which follow narrow mountain ranges at both margins of the Dasht-e-Lut desert. East of the Dasht-e-Lut, right-lateral faulting runs through the Sistan suture zone (Tirrul *et al.* 1983). North of 34°, E–W left-lateral faulting predominates. Box shows the location of Fig. 2.

Arabia–Eurasia convergence (Sella *et al.* 2002). Local GPS studies suggest that between a third and a half of Arabia–Eurasia shortening (*ca* 10–12 mm yr^{-1}) is taken up in the central Zagros (Tatar *et al.* 2002; Hessami 2002). Therefore *ca* 15–20 mm yr^{-1} of shortening at 60°E remains to be accommodated in central Iran and the Alborz, causing an equal amount of N–S right-lateral shear in eastern Iran.

We believe that the present-day tectonic configuration in Iran dates from *ca* 5 Ma. This time marks the onset of deformation across much of the broader collision zone. Major deformation of the Zagros folded belt dates from the Pliocene, *ca* 5 Ma or less (Falcon 1974). A major reorganization of the sedimentation and deformation in the south Caspian basin also occurs at about this time (Devlin *et al.* 1999; Jackson *et al.* 2002). If the present-day active faults date from this time, we would therefore expect a total of *ca* 75–100 km of right-lateral shear between Iran and Afghanistan.

South of 34°N, this right-lateral shear is accommodated on north–south right-lateral strike-slip faults to the east and west of the Lut desert (the Dasht-e-Lut, Fig. 1c). North of 34°N, the dominant structures are the Doruneh and Dasht-e-Bayaz left-lateral strike-slip faults, which are thought to accommodate right-lateral shear by rotating clockwise, away from the direction of maximum shortening (Fig. 1c; Jackson & McKenzie 1984; Jackson *et al.* 1995). Similar rotations have been suggested for strike-slip faults in eastern Tibet (England & Molnar 1990; Holt *et al.* 1991).

We focus on the Dasht-e-Bayaz fault system (Figs 1c and 2). This is north of the active right-lateral faults of the Sistan suture zone (the Neh and Abiz fault systems, Fig. 1c; Berberian *et al.* 1999, 2000), which may accommodate a large proportion of the *ca* 20 mm yr^{-1} right-lateral shear between Iran and Afghanistan (Tirrul *et al.* 1983; Walker & Jackson 2002). We might expect therefore that the

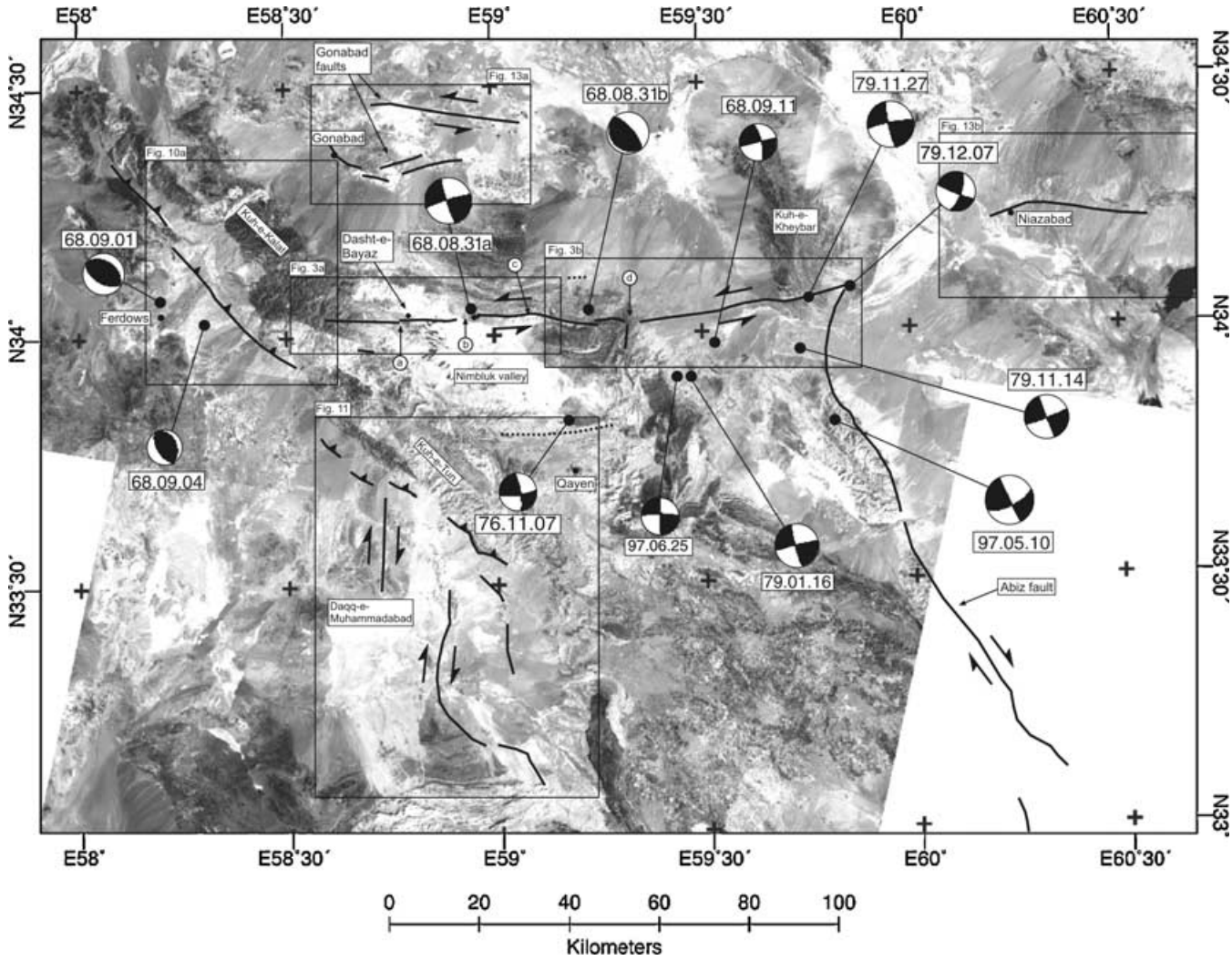

Figure 2. LANDSAT mosaic of the Dasht-e-Bayaz region. Holocene and coseismic fault scarps are represented as thin black lines. Fault-plane solutions are from long-period body wave inversion. Solutions for the 1968 August 31 and 1979 September 27 events are from this paper, the others are from various sources (see Table 2). Relocated epicentres are from Engdahl *et al.* (1998). Circled letters (a to d) represent left-steps in the 1968 coseismic faulting (Ambraseys & Tchalenko 1969; Tchalenko & Berberian 1975). Boxes show the location of later figures.

Table 1. Historical earthquakes in the Dasht-e-Bayaz region. Details are taken from: (1) Ambraseys & Melville (1982), (2) Berberian & Yeats (1999), (3) Berberian & Yeats (2001), (4) Berberian *et al.* (1999) and (5) Ambraseys & Tchalenko (1969).

Date	Time	Location	Mag.	Ref.	Fault
AD856 December	?	Widespread damage	?	5	Several?
AD1066 May	?	Qayen	?	2, 3	?
1238	?	Gonabad	?	2, 3	Gonabad/Bidokht? (Fig. 12a)
1549 February 15	?	E. Qayen/Birjand	*ca* 6.7	1, 4	N. Birjand (Fig. 1c)
1675 Winter	?	Gonabad	?	2, 3	Gonabad/Bidokht? (Fig. 12a)
1847	?	Qayen	?	4	?
1923 November 29	?	S.E. of Qayen	5.6	4	?
1936 June 30	?	Abiz	6	4	Abiz (Fig. 2)
1941 February 16	Late evening	Muhammadabad	?	1	Chahak (Fig. 10)
1947 September 23	Morning	Dustabad	?	1	Dustabad (Fig. 10)
1962 April 1	Dawn	Musaviyeh	?	1	Chahak? (Fig. 10)

Table 2. Instrumentally recorded earthquakes for the Dasht-e-Bayaz region that have been modelled using body waves. 'm' in the M_w column signifies a multiple event. These fault-plane solutions are shown on Fig. 2. Epicentres are from Engdahl *et al.* (1998). References are: (1) Baker (1993), (2) Berberian *et al.* (1999), (3) Walker *et al.* (2003), (4) Jackson (2001), (5) this paper.

Date	Time	Lat.	Long.	Depth	M_w	Strike	Dip	Rake	Ref.	Fault
1968 August 31	10:47	34.05	58.95	17	7.10	254	84	5	5	W. D-e-Bayaz
1968 August 31	10:47	34.05	*ca* 59.25	10	6.44	320	70	90	5	W. D-e-Bayaz
1968 September 1	07:27	34.07	58.21	9	6.25	115	54	85	3	Ferdows
1968 September 4	23:24	34.03	58.31	9	5.48	148	56	81	3	Ferdows
1968 September 11	19:17	33.97	59.53	6	5.6	78	90	16	1	D-e-Bayaz
1976 November 7	04:00	33.83	59.18	8	6.03 m	84	79	12	1,4	Qayen
1979 January 16	09:50	33.91	59.47	11	6.48 m	162	66	115	1, 4	Qayen
1979 November 14	02:21	33.96	59.73	10	6.57 m	160	89	−177	1, 4	Abiz
1979 November 27	17:10	34.06	59.76	8	7.1	261	82	8	5	E. D-e-Bayaz
1979 December 7	09:23	34.08	59.86	10	5.9	113	84	21	1	Abiz
1997 May 10	07:57	33.81	59.81	13	7.12	156	89	−160	2	Abiz
1997 June 25	19:38	33.91	59.44	8	5.7	181	87	170	2	Boznabad

ca 200 km long Dasht-e-Bayaz fault rotates relatively rapidly (up to *ca* 6° per Myr, if it is pinned at its eastern end, where it abuts stable Afghanistan, and if it accommodates 20 mm yr^{-1} of right-lateral shear) and this may be reflected in the style and scale of tectonic features associated with it.

3 ACTIVE FAULTING ON THE DASHT-E-BAYAZ FAULT

3.1 Seismicity

The Dasht-e-Bayaz region has suffered several large 20th century earthquakes and abundant historical activity. The distribution of destructive earthquakes gives insight into the patterns of active deformation in the Dasht-e-Bayaz region. The modelling of earthquake source parameters using instrumentally recorded seismic body waves also gives detailed information about the distribution of faulting on short time-scales, and the nature of this faulting at depth. In this section we summarize the historical and instrumental seismic activity, and also determine source parameters for the two largest instrumentally recorded earthquakes (1968 August 31 and 1979 November 27), which, between them, have ruptured the entire *ca* 120 km length of the Dasht-e-Bayaz fault zone.

3.1.1 Historical earthquakes

Iran has a long historical record and several authors have compiled catalogues of earthquake activity from historical texts. The reported historical earthquakes for the Dasht-e-Bayaz region are summarized in Table 1, and are discussed in detail by Ambraseys & Tchalenko (1969), Ambraseys & Melville (1982), Berberian & Yeats (1999, 2001) and Berberian *et al.* (1999). All the pre-20th century earthquakes in Table 1 are based on reports of damage distributions, and cannot be assigned with certainty to individual faults. However, damage in the AD1238 and AD1675 events was restricted to the Gonabad region (Berberian & Yeats 2001), indicating a probable rupture nearby (Fig. 2). Reports of widespread damage in AD856 December are vague and may refer to several destructive earthquakes across the Khorassan province of NE Iran (Ambraseys & Tchalenko 1969). Surface ruptures have been attributed to 20th century events in 1936, 1941, 1947, and 1962 (Ambraseys & Melville 1982; Berberian *et al.* 1999), although the surface ruptures were not visited until years after the earthquakes.

3.1.2 Instrumentally recorded earthquakes

The late 20th century sequence of earthquakes on the Dasht-e-Bayaz and Abiz fault systems has been summarized by Berberian & Yeats (1999) and Berberian *et al.* (1999). The source parameters of the earthquakes are summarized in Table 2, including the source parameters of the 1968 August 31 and 1979 November 27 earthquakes determined in this study by analysis of long-period body-waves. These earthquakes are discussed in the following sections.

3.2 Source parameters of instrumentally recorded earthquakes

We used body waveforms to constrain the source parameters of the 1968 August 31 and the 1979 November 27 earthquakes. Paper seismogram records for stations of the WWSSN network in the epicentral range of 30–90° were digitized. We then used the MT5 version (Zwick *et al.* 1995) of McCaffrey & Aber's (1988) and McCaffrey *et al.*'s (1991) algorithm, which inverts the *P* and *SH* waveform data to obtain the strike, dip, rake, centroid depth, seismic moment and source time-function. We always constrained the source to be a double-couple. The method and approach we used are described in detail elsewhere (e.g. Nabelek 1984; Taymaz *et al.* 1991) and are now too routine to justify repetition here.

3.2.1 The 1968 August 31 Dasht-e-Bayaz earthquake

This M_w 7.1 earthquake produced *ca* 80 km of surface ruptures, from longitude *ca* 58°35′E (Fig. 3a) to east of Zigan, at longitude *ca* 59°25′E (Fig. 3b), and caused extensive damage in the region, particularly in the Nimbluk valley (Figs 2 and 3a), where many villages were completely destroyed (Tchalenko & Ambraseys 1973; Ambraseys & Melville 1982). Between 7000 and 12 000 people were killed and at least 70 000 made homeless (Ambraseys & Tchalenko 1969). Maximum left-lateral offsets of *ca* 4.5 m and maximum vertical displacements of *ca* 2.5 m were observed, with average displacements of *ca* 2 m (Ambraseys & Tchalenko 1969).

The *P* waveforms for the Dasht-e-Bayaz main shock are complicated, and many of the *SH* waves were off scale on the old WWSSN long-period instruments (Fig. 4). Visual inspection of the seismograms reveals a number of important features. For the *P* waves, northern stations Q-S all have relatively small amplitudes and so are likely to be near a nodal plane, and all the stations in the arc

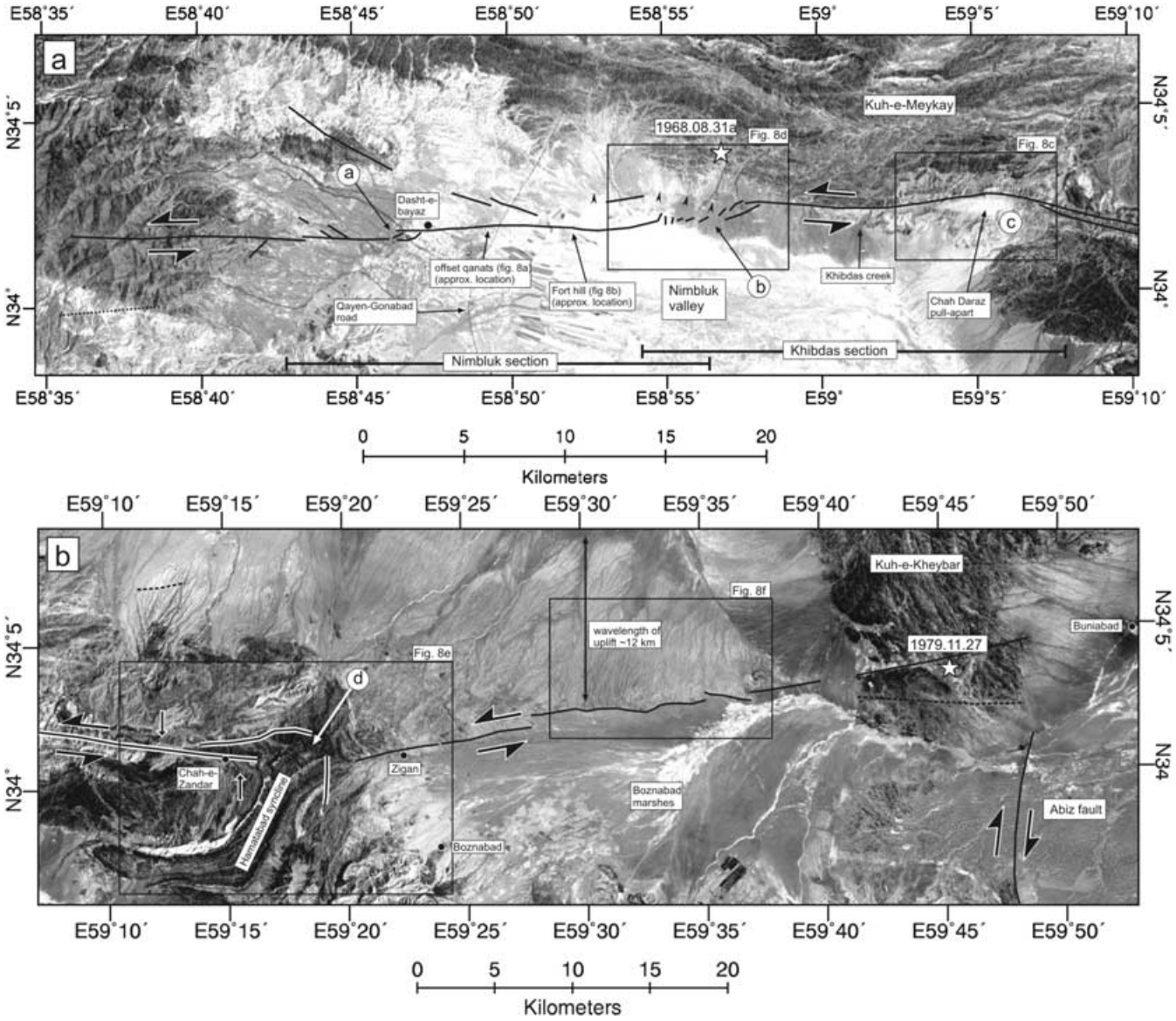

Figure 3. (a) ASTER image of the western part of the 1968 August 31 ruptures in the Nimbluk valley (see Fig. 2 for location). Ruptures of the 1968 August 31 earthquake extend eastwards onto Fig. 3(b). Ruptures are drawn from Berberian (1976), which are redrawn from Ambraseys & Tchalenko (1969), Tchalenko & Ambraseys (1970) and Tchalenko & Berberian (1975). In the eastern half of the image, coseismic ruptures occur within bedrock of Kuh-e-Meykay. The lithologies are different across the fault. West of 59°E, the faulting steps *ca* 1 km to the south (marked b), and can be traced along the floor of the valley. Left-steps in faulting also occur at points marked a and c. Clear Holocene scarps run along the northern margin of the valley (marked with black arrows), short sections of these were reactivated in 1968. The Nimbluk and Khibdas sections (Ambraseys & Tchalenko 1969; Tchalenko & Berberian 1975) are indicated at the bottom of the figure. Boxes show the location of later figures. (b) LANDSAT image of the eastern part of the Dasht-e-Bayaz fault. Ruptures of the 1968 August 31 earthquake extend from the western end of the image to east of Zigan, the 1979 ruptures were from Chah-e-Zander to Buniabad. Faults are drawn from Berberian (1976), Behzadi (1976), Haghipour & Amidi (1980) and our own analysis of the satellite imagery. Lithologies apparently displaced by *ca* 5–6 km by the fault near Chah-e-Zander are marked with black arrows. Cumulative scarps in the Boznabad marshes are south-facing, with uplifted NE grading fans on their northern flanks.

from northwest to east show a double pulse at the start of the *P* waveform. The shape of the pulses in east and west directions are quite similar, but relatively compressed in the east (compare HKC with COP), which suggests that the rupture propagated from west to east (see e.g. Berberian *et al.* 1999). The available *SH* waveforms, which fortunately cover a wide range of azimuths, are all relatively simple (Fig. 4). There is little doubt that the main moment release in this earthquake involved east–west left-lateral strike-slip faulting, because of the observed surface rupture. In addition, the long-period first motion polarities provide a well-constrained orientation of the early part of the rupture (McKenzie 1972) that is in agreement with the surface ruptures.

A free inversion of the long-period waveforms produces a strike-slip solution that is compatible with both the first motion polarities and the surface faulting (solid nodal planes in Fig. 4). To obtain this solution, we parametrized the source time-function using triangles of half-duration (τ) 2 s, which was necessary to obtain a time-function of sufficient overall duration, but consequently we cannot hope to match all the higher-frequency details of the *P* waveforms. The time-function duration is *ca* 18 s, which gives a fault length of *ca* 60 km

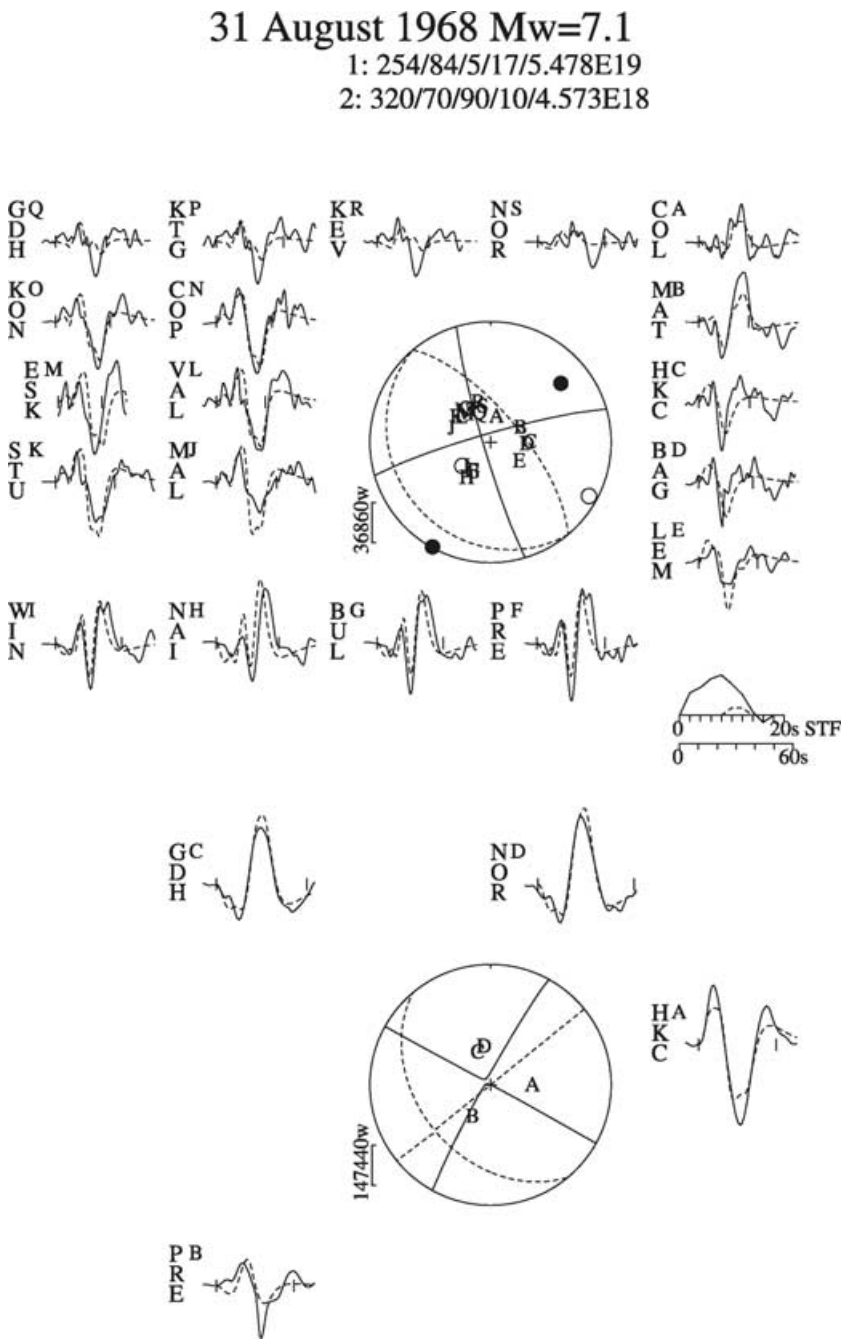

Figure 4. Final inversion result for the 1968 August 31 Dasht-e-Bayaz earthquake. Waveforms are digitized from paper WWSSN records. Solid nodal planes represent a free inversion of the long-period waveforms, dotted nodal planes represent a separate subevent with thrust mechanism *ca* 8 s after the initial onset. The high frequency content of the *P*-wave seismograms is probably caused by several subevents that we cannot match in our inversion (see text for full discussion).

with a typical rupture velocity of *ca* 3.5 km s^{-1}, which is close to the observed *ca* 80 km length of the coseismic surface ruptures. However, this strike-slip solution is not wholly satisfactory for two reasons. First, because of the double pulse in the *P* wave onsets (clearest at western stations such as KON, COP), the inversion is led to a depth of *ca* 17 km. This is inevitable because, at all the western stations, the pP pulse is small and down, while sP is large and up. It is much more likely that the true centroid was shallower (typically *ca* 8 km eastern Iran; see Berberian *et al.* 1999). With a seismogenic thickness of 15 km, the observed moment (*ca* 5.9 × 10^{19} N m) and fault length (*ca* 60 km) gives an average slip value of *ca* 2.2 m, which is close to that observed. A centroid depth of 17 km would double the seismogenic thickness and halve the average slip. It is likely that the double pulse comes from a second subevent, whose details we are unable to resolve, and that the centroids of all the subevents of this complicated rupture were relatively shallow. For these large earthquakes, with long time-functions, some trade-off between centroid depth and time-function duration is anyway inevitable. Secondly, the strike-slip solution alone is unable to match the waveforms at southern stations F-I (see station WIN in Fig. 5, line

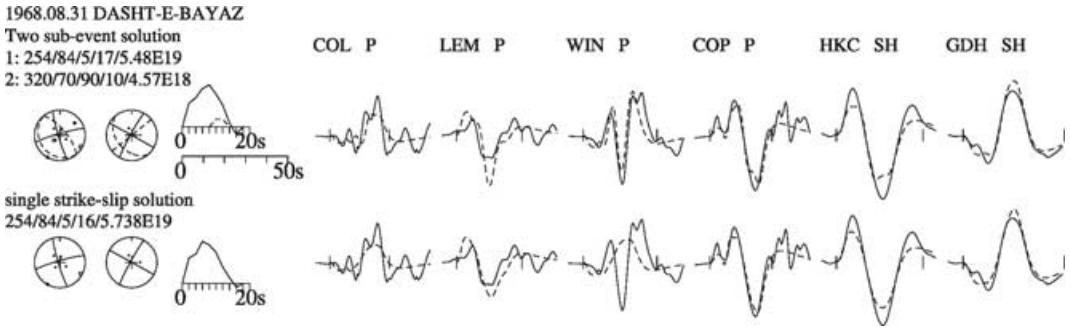

Figure 5. Comparison of our two-subevent solution (line 1) with a solution involving a single strike-slip event (line 2). The strike-slip solution is unable to match the *P* waveforms for southern stations (e.g. WIN). The addition of a later pulse with thrust mechanism (line 1), improves the fit at southern stations, without degrading the fit of *P* and *SH* waveforms at other stations. See text for full discussion.

2). All these southern stations have similar waveforms, suggesting that they reflect real source effects, including a large inverted w-shaped pulse at *ca* 10 s into the waveform that is not present at other azimuths. Such a pulse cannot be caused by the strike-slip rupture, as it is too late, is of the wrong polarity for the surface-reflected phases, and doesn't affect stations at other azimuths.

The extra pulse at southern stations can be matched by including a separate, relatively small (M_w 6.4) subevent 8 s after the initial onset, with a mechanism involving thrusting with a NW–SE strike and a steep (70°) NE-dipping nodal plane (Fig. 4, dashed nodal planes). This produces a reasonable fit to the southern waveforms at stations F-I without degrading the fits of *P* and *SH* waves at other stations (see Fig. 5). Thrusting of this orientation is seen throughout this part of eastern Iran (e.g. Berberian 1976; Walker *et al.* 2003) and would not be surprising. We placed the epicentre of this subevent 24 km east of the main shock, but neither this, nor its orientation are well resolved.

We conclude that about 90 per cent of the moment in this earthquake was released in the roughly E–W left-lateral strike-slip faulting that produced the surface ruptures, though probably in several subevents whose details we are unable to resolve. However about 10 per cent of the moment may have been associated with a subevent involving thrusting.

The relocated epicentre of this earthquake is at 34°3.1′N 58°57′E (Engdahl *et al.* 1998), placing it approximately mid-way along the surface rupture, but displaced *ca* 8 km to the north of the ruptures. Instrumental epicentres in eastern Iran are in error by up to 10 km and are typically NE of their true epicentres (Berberian 1979; Ambraseys 2001). It therefore seems reasonable that the earthquake nucleated along the line of surface ruptures, possibly at the pull-apart basin marked b in Figs 2 and 3(a), which is *ca* 5 km SW of the relocated epicentre (Fig. 3a).

3.2.2 The 1979 November 27 Khuli-Buniabad earthquake

This large event of M_w 7.1 produced *ca* 60 km of surface ruptures along the eastern part of the Dasht-e-Bayaz fault, from longitude *ca* 59°15′E to 59°50′E, between the villages of Chah-e-Zandar and Buniabad (Figs 2 and 3b; Haghipour & Amidi 1980; Ambraseys & Melville 1982). This earthquake apparently re-ruptured the easternmost *ca* 10 km of surface faulting in the 1968 Dasht-e-Bayaz event, which continued east of Zigan (Fig. 3b; Ambraseys & Tchalenko 1969). The region is sparsely populated and the earthquake caused relatively few deaths (Ambraseys & Melville 1982). Surface ruptures were not investigated in detail at the time, but Haghipour & Amidi (1980) report vertical offsets of up to 2.5 m and left-lateral horizontal displacements of 1–4 m. At the eastern end of the rupture. Haghipour & Amidi (1980), report that the northernmost *ca* 10 km of the Abiz right-lateral fault was also reactivated in this earthquake, but Berberian *et al.* (1999) identify the 1979 December 7 Kalat-e-Shur earthquake (Table 2) as being responsible for these ruptures. The relocated epicentre is at 34°3.5′N 59°45.4′E (Engdahl *et al.* 1998). This is at the eastern end of the 1979 surface ruptures and indicates a westward propagation.

The waveforms for this event are rather similar to those of the 1968 Dasht-e-Bayaz main shock (compare Figs 6 and 4). Once again, there is no doubt that the main rupture involved east–west left-lateral strike-slip faulting, because of the observed surface ruptures. Again we parametrized the source time-function with elements of (τ) = 2 s, and obtained a solution compatible with both the surface ruptures and the first motion polarities (Jackson & McKenzie 1984). The synthetic seismograms reproduce the main features of the observed waveforms but, as before, cannot match some of the higher-frequency details with the time-function parametrization we used. There is some hint of an anomalous pulse at south stations GRM and PRE in Fig. 7, as before (see Fig. 4), but not at the adjacent stations BUL and NAI, so we did not attempt to include another subevent. As with the 1968 Dasht-e-Bayaz main shock (Fig. 4), the higher-frequency details in the *P* waves make it probable that the strike-slip rupture occurred in several discrete subevents. Note that in Fig. 6 the inversion has matched the double upward pulse at western stations by a discrete pulse (in effect, a separate subevent) in the source time-function. We believe this is also likely to be the correct explanation for the similar pulse observed in the 1968 main shock, discussed earlier (Section 3.2.1, Fig. 4). The overall stability of the solutions for both the 1968 and 1979 main shocks is anchored by the simple SH waveforms, particularly the near-nodal stations LEM in Fig. 6 and PRE in Fig. 4. If we assume a seismogenic thickness of 15 km and a fault length of 60 km, the moment of 5×10^{19} N m would give an average slip of 1.85 m in the 1979 main shock, which is comparable to that observed at the surface (Haghipour & Amidi 1980).

A Harvard CMT solution is available for the 1979 main shock, and differs significantly only in the dip (by 15°) and rake (by 27°), giving the rupture a normal component. We carried out an inversion with the strike, dip and rake fixed to the Harvard values and the depth fixed to 8 km, but with the time-function and moment free. The Harvard solution (Fig. 7, line 2) shows a general degradation of fit to the P waveforms, particularly at stations to the south (e.g. NAI), which are no longer close to a nodal plane. The *SH* waveforms are relatively unaffected.

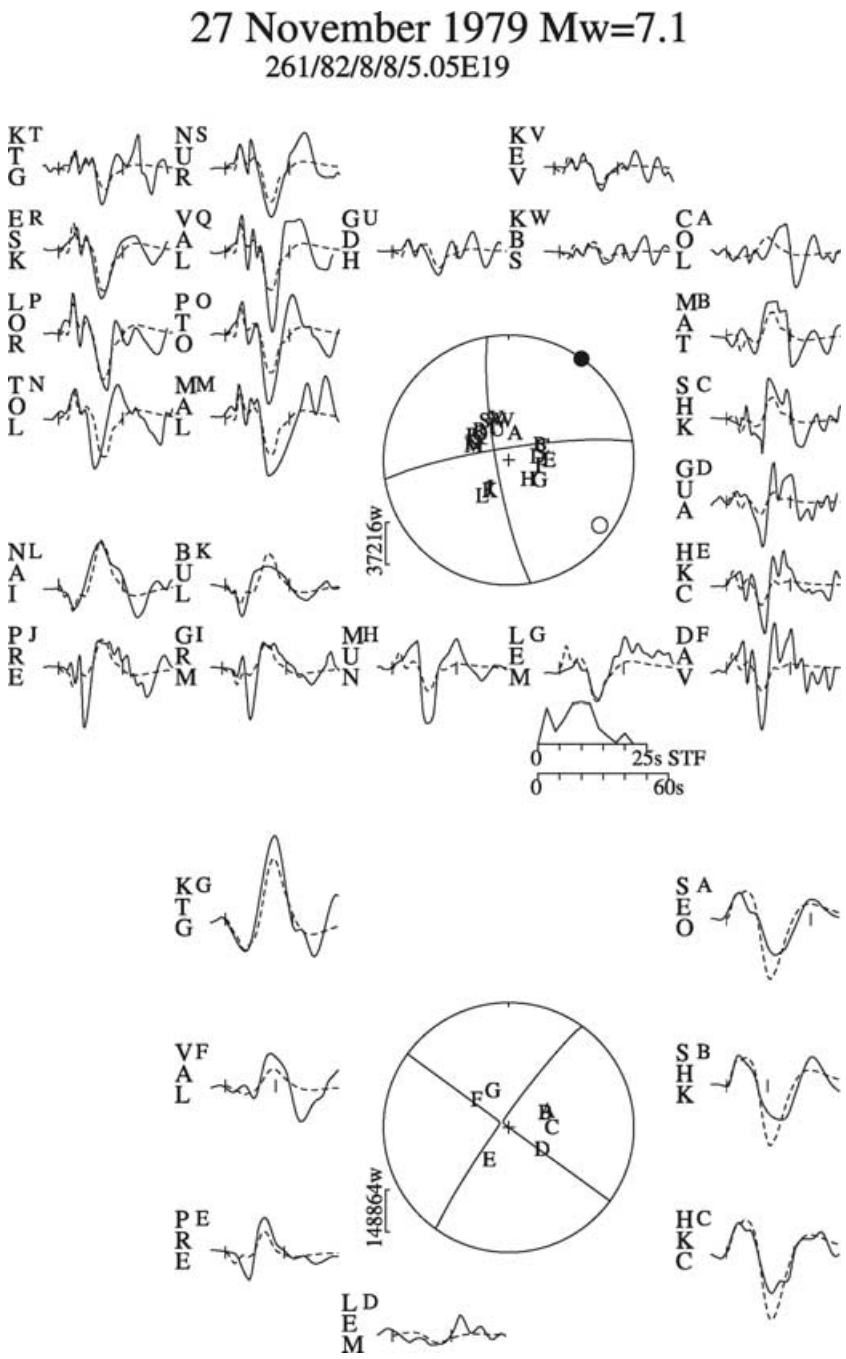

Figure 6. Final inversion result for the 1979 November 27 Khuli-Buniabad earthquake. Waveforms are digitized from paper WWSSN records. Like the 1968 Dasht-e-Bayaz earthquake (Fig. 4), high frequency content in the *P*-wave seismograms suggests several discrete subevents. See text for full discussion.

Coseismic (Haghipour & Amidi 1980) and cumulative scarps (Figs 2 and 3b) show uplift north of the fault, which may indicate a slight reverse component of slip, from the almost vertical fault plane indicated by the solution. Alluvial fans are incised by streams for *ca* 12 km north of the fault (Fig. 3b), which probably represents the limit of cumulative surface uplift. The wavelength of surface deformation away from the fault is expected to be roughly similar to the depth to which the fault extends. Thus the observed wavelength of *ca* 12 km is compatible with the *ca* 8 km centroid depth determined here.

3.3 Geomorphic and coseismic surface expression of the Dasht-e-Bayaz fault

Information from earthquake surface ruptures and the geomorphology of the fault zone can be combined with earthquake source parameters to show the segmented structure of the Dasht-e-Bayaz fault. Segmentation of the fault is important if the faults are rotating clockwise about a vertical axis, as the segments may rotate independently, and hence disrupt the continuity of the fault. We show below that the pattern of deformation recorded in recent earthquakes cannot

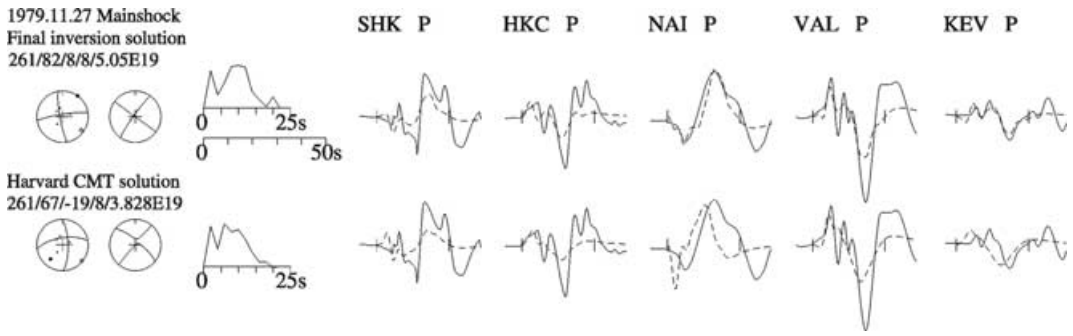

Figure 7. A comparison between our final inversion solution (line 1) and an inversion using fixed values of strike, dip and rake of the Harvard CMT solution and a fixed depth of 8 km (line 2). The Harvard source parameters lead to a general degradation in fit to *P* waves (particularly at NAI). See text for full discussion.

account for the overall geomorphology of the fault system, and the faults must be evolving in response to clockwise rotation. This has implications for the role of the Dasht-e-Bayaz region in accommodating the right-lateral shear between Iran and Afghanistan (Fig. 1c).

We consider the western and eastern parts of the fault separately, as they ruptured in separate large earthquakes in 1968 and 1979 (see Table 2 and Fig. 2).

3.3.1 The western Dasht-e-Bayaz fault

This part of the fault (from the western end of the fault to just east of point d on Figs 2 and 8b), which ruptured in the 1968 August 31 Dasht-e-Bayaz earthquake, was studied in detail at the time. There is abundant evidence of Holocene left-lateral slip along the earthquake rupture, with stream channels offset by 8–28 m. The clearest of these is at Khibdas creek (Fig. 5a; Berberian & Yeats 1999). Ancient qanats (underground canals) are offset by *ca* 10 m across the fault (Figs 3a and 8a; Ambraseys & Tchalenko 1969). Assuming a maximum age of *ca* 4000 yr for these tunnels (which is the age of the oldest recorded qanat in Iran; Mehryar & Kabiri 1986), a minimum slip-rate of *ca* 2.5 mm yr^{-1} is determined (Berberian & Yeats 1999). However, these qanats are likely to be much younger than *ca* 4000 yr (Ambraseys, private communication, 2003), and may indicate a higher rate of slip. As stated earlier, the Dasht-e-Bayaz fault is expected to rotate clockwise by up to 6° per Myr. Fault slip-rates caused by this rotation will vary with the width of the rotating fault-bounded blocks, but for blocks of *ca* 100 km width, which seems a sensible scale (Fig. 2), this rotation would result in a slip-rate of *ca* 1 cm yr^{-1} (see Fig. 9). However, the rigid-block rotations in Fig. 9 are a simplification, as the rotations must involve internal deformation of the blocks (as discussed later).

There are apparently only small cumulative offsets of bedrock lithologies across the fault, with estimates from *ca* 400 m to 4 km (Tchalenko & Berberian 1975). Offset lithologies are difficult to see on satellite imagery, although one distinctive unit of Palaeocene–Eocene micrite appears to be displaced across the fault by *ca* 5–6 km (Figs 3b and 8e; Alavi-Naini 1983). The *ca* 2.5 km length of the Chah Daraz pull-apart basin suggests a small cumulative fault offset (Figs 5a and 8c). The faulting does not displace the Kuh-e-Meykay mountain range-front (east of point d on Fig. 3b) by any appreciable amount, which might be expected if the total cumulative displacements are large. A simple calculation (see Fig. 9) shows that an offset of *ca* 4 km achieves a N–S right-lateral shear of *ca* 8 km.

Fig. 3 shows detailed surface ruptures of the 1968 earthquake, mapped by Ambraseys & Tchalenko (1969), who separate the ruptures into the Nimbluk (west) and Khibdas (eastern) sections (see Fig. 3a). The eastward continuation of faulting was not mapped in the same detail. These two sections are separated by a *ca* 4 km gap in the 1968 coseismic ruptures and a left-step of *ca* 1 km in the faulting (Tchalenko & Berberian 1975), shown as gap b in Figs 3(a) and 8(d). Given the uncertainty in epicentral location, the earthquake may have nucleated at this gap. A further left-step in the coseismic ruptures occurred *ca* 1 km west of Dasht-e-Bayaz village (gap a in Fig. 3a), although this did not show the same reduction in slip.

Within the Nimbluk valley, the surface ruptures cut through alluvium with subdued geomorphology. Low hills and small stream displacements are too subtle to be seen in our satellite imagery, but are clear in aerial photos (e.g. Figs 8a and b). Larger cumulative south-facing scarps are present along the northern margin of the valley, but only small sections of these were reactivated in 1968 (Figs 3a and 8d). However, these cumulative scarps are directly aligned with the 1968 Khibdas section ruptures (Figs 3 and 8d), and may represent a now abandoned western continuation of the Khibdas fault segment. The possible significance of these abandoned scarps is discussed later.

The Khibdas section of Ambraseys & Tchalenko (1969) runs eastward into the Kuh-e-Meykay mountains (Fig. 3a). The ruptures are uninterrupted for *ca* 30 km to *ca* 59°15′E, where another segment break occurs (gap d in Figs 2 and 3b). Bedding within the Hamatabad syncline (Figs 3b and 8e) is not displaced by faulting, but coseismic and cumulative scarps occur immediately to the east and west. A zone of north–south right-lateral faulting occurs in the gap between segments. The 1969 ruptures continued eastwards into the Boznabad marshes east of Zigan (Fig. 3b; Ambraseys & Tchalenko 1969).

3.3.2 The eastern Dasht-e-Bayaz fault

The eastern part of the Dasht-e-Bayaz fault ruptured in 1979, producing 50–60 km of surface ruptures. These were mapped by Haghipour & Amidi (1980), but the published fault maps are not detailed. Cumulative south-facing scarps are clearly seen on LANDSAT imagery (Figs 3b and 8f), these appear to be relatively discontinuous (Fig. 8f). The cumulative scarps cut alluvium and show incision of fan systems that were originally deposited by streams flowing to the NNE, but which are now deflected eastwards around the southern margin of Kuh-e-Kheybar (Fig. 3b).

The 1979 ruptures extend eastwards into Kuh-e-Kheybar (Fig. 3b). Haghipour & Amidi (1980) identify a rupture that curves slightly to the north, and appears to displace the eastern margin of Kuh-e-Kheybar by 3–4 km left-laterally. A possible southerly fault branch is also identified on LANDSAT imagery (the dotted line on Fig. 3b), but does not appear to displace lithologies by any appreciable amount. The eastern end of the ruptures seem to join with the north–south right-lateral Abiz fault. Although there is little apparent

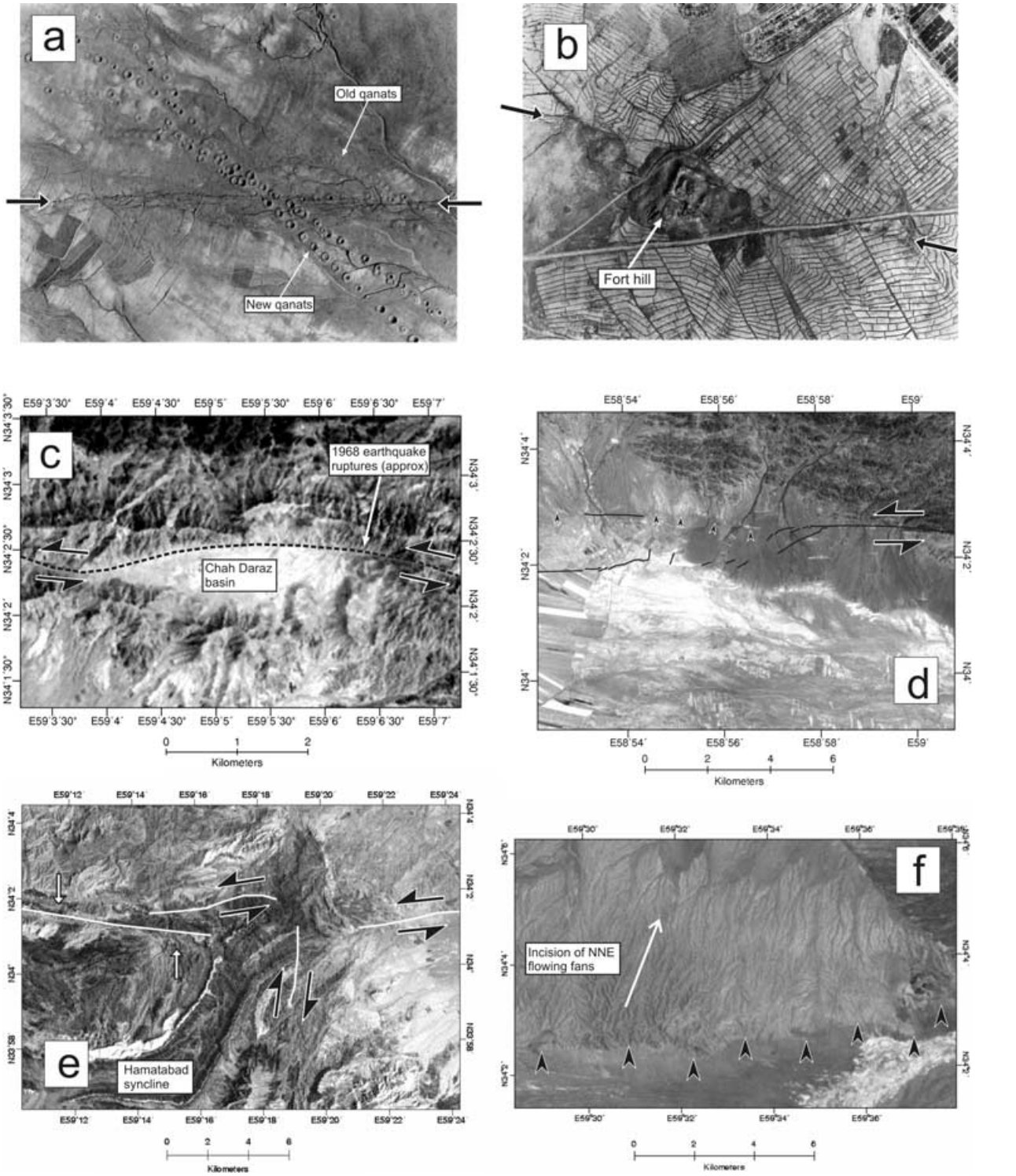

Figure 8. Close-up views of tectonic features on the Dasht-e-Bayaz fault. See Fig. 3 for locations. (a) 1:7500 aerial photo taken after the earthquake. The shafts of underground canals (qanats) are displaced across the fault by up to 10 m (Ambraseys & Tchalenko 1969). Several generations of qanat indicate repeated disruption to the water flow. One branch follows the fault plane. (b) 1:7500 aerial photo taken after the earthquake. Cumulative Holocene displacements in the form of a small push-up (Fort hill) can be seen. These features are too small to be seen on ASTER and LANDSAT imagery. (c) ASTER view of the Chah Daraz valley. This is bounded on its northern side by the fault, and seems to be a small pull-apart basin. It is *ca* 2.5 km long. (d) ASTER image of the left-step in 1969 coseismic ruptures at *ca* 59°E. Coseismic displacements decreased to zero in the region of this step-over. A series of south-facing cumulative scarps (marked by black arrows) was not reactivated in 1969, apart from along small sections. (e) LANDSAT view of the segment boundary near Boznabad. Beds within the Hamatabad syncline are not displaced left-laterally, the 1968 coseismic ruptures are discontinuous, and right-lateral faulting occurs in the gap. In the west of the image, Tertiary micritic sediments (Alavi-Naini 1983) are displaced by 5–6 km left-laterally in the fault zone (these appear as dark rocks in the satellite image and are marked by vertical black arrows). (f) LANDSAT view of cumulative scarps along the 1979 earthquake rupture. They are formed in alluvium, appear discontinuous and interrupt NE flowing drainage.

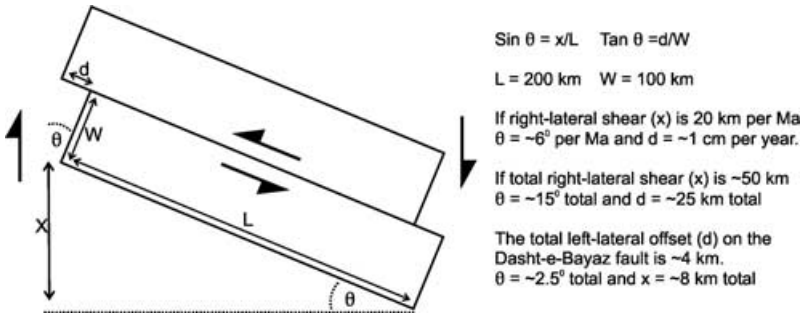

Figure 9. Cartoon showing how N–S right-lateral shear can be accommodated by clockwise rotation about vertical axes of blocks with left-lateral strike-slip faults at their edges. This model does not account for internal deformation within the fault-bounded blocks (which must occur, see Fig. 14b), but is a useful approach for determining the fault displacements caused by N–S right-lateral shear. The total left-lateral offset (d) on these faults depends not only on the amount of N–S right-lateral shear (x) but also on the length (L) and width (W) of the blocks. The clockwise rotation (θ) can be expressed in terms of these dimensions. We use values of 200 km and 100 km for L and W, which seem sensible (Fig. 2). Although the calculated values of d and θ are not precise, as we have assumed values of L and W, they provide an estimate that can be compared to observed values of d and θ. The three calculations described at right refer to situations discussed in the text.

deformation in the region between the two faults, this is not a stable configuration and is likely to evolve rapidly.

3.3.3 Active faulting on the Dasht-e-Bayaz fault: a summary

In summary, although the Dasht-e-Bayaz fault has generated several large, destructive earthquakes and may have a slip-rate of greater than *ca* 2.5 mm yr^{-1}, it appears that the total E–W left-lateral cumulative offset across the fault is only a few kilometres, which can in turn account for $<$20 km of N–S right-lateral shear (following from the simple model in Fig. 9). The fault is highly segmented, with small pull-aparts formed at the segment ends. The fault is clearly evolving rapidly, with the abandonment of cumulative scarps near the segment ends. The distinctive structure and geomorphology of the Dasht-e-Bayaz fault is probably related to its role in accommodating right-lateral shear between Iran and Afghanistan. The implications of this for the regional tectonics are a major aim of this paper and are discussed later.

4 DISTRIBUTED FAULTING AROUND THE DASHT-E-BAYAZ FAULT

Below, we use simple observations of the geomorphology and seismicity to describe the active faulting and folding in the regions around the Dasht-e-Bayaz fault. We show that distributed strike-slip and thrust faulting is widespread. It is possible that the Dasht-e-Bayaz fault, rather than being a single through-going structure, may be composed of several of these independent, short fault segments that influence each other due to their alignment, and may eventually coalesce.

4.1 The Ferdows thrust fault

Walker *et al.* (2003) usomorphology east of Ferdows (Fig. 2) to show a zone of uplifted and folded late Tertiary and Quaternary sediments formed above an eastward dipping thrust fault. They relate this zone of deformation to two thrust earthquakes on 1968 September 1st and 4th (Fig. 10 and Table 2), shortly after the Dasht-e-Bayaz earthquake. Present-day folding and faulting appears to have migrated westwards into the footwall of an older (Neogene) thrust fault, which forms the Kuh-e-Kalat range front (Fig. 10; Walker *et al.* 2003). Coseismic surface ruptures of the 1968 August 31 left-lateral strike-slip earthquake extend westwards to the southeastern end of Quaternary folding associated with the Ferdows thrust fault (Fig. 2). Uplift above the Ferdows fault appears greatest at its southeastern end, where Quaternary and Neogene sediments have been stripped away leaving bedrock exposure (Fig. 10a). The two structures are probably linked, and displacements on the Ferdows thrust fault decrease away from the intersection.

A westward migration of thrust faulting at Ferdows may be contributing to the growth of the Dasht-e-Bayaz strike-slip fault zone, as the strike-slip fault grows to link with the new, more westerly thrust fault. A similar mechanism has been suggested for the growth of strike-slip faults in Mongolia (Bayasgalan *et al.* 1999) and Tibet (Meyer *et al.* 1998).

4.2 The Muhammadabad fault system

The Ferdows thrust fault appears to branch northwards from the western end of the Dasht-e-Bayaz fault, with displacement that dies away with distance from its junction with the Dasht-e-Bayaz fault. However, there are several indications of folding (and blind thrust faulting) parallel and to the west of the Kuh-e-Tun mountain range south of the intersection with the Dasht-e-Bayaz fault (Figs 2 and 11). At least three north–south oriented faults occur around the Daqq-e-Muhammadabad (a flat, encrusted, internally draining basin, see Fig. 11). Below, we discuss these faults and the evidence that they reactivate parts of the Kuh-e-Tun range at their ends.

4.2.1 The Dustabad fault

This is situated north of the Daqq-e-Muhammadabad. The southern part of the fault runs through bedrock mountains and is not visible on LANDSAT TM+ imagery. This part ruptured in the 1947 September 23 Dustabad earthquake (Fig. 11 and Table 1). Coseismic ruptures (identified by local people) were visited by Ambraseys and Melville in 1978 (Ambraseys & Melville 1982). The ruptures ran as discontinuous cracks for *ca* 20 km trending 350°. Right-lateral offsets of *ca* 1 m were seen in several localities. Vertical offsets of 30–80 cm were also noted. Local information suggests that ground deformations continued northwards into the alluvial plain to Istakhr (Fig. 11). Although this information cannot be verified, a zone of folding runs northwestwards from the vicinity of Ishtakhr (Figs 11 and 12a), and the two structures may be linked in some way.

4.2.2 The Chahak fault

An *ca* 30 km long north–south fault, runs along the eastern margin of the Daqq-e-Muhammadabad (Fig. 11). A clear Holocene scarp

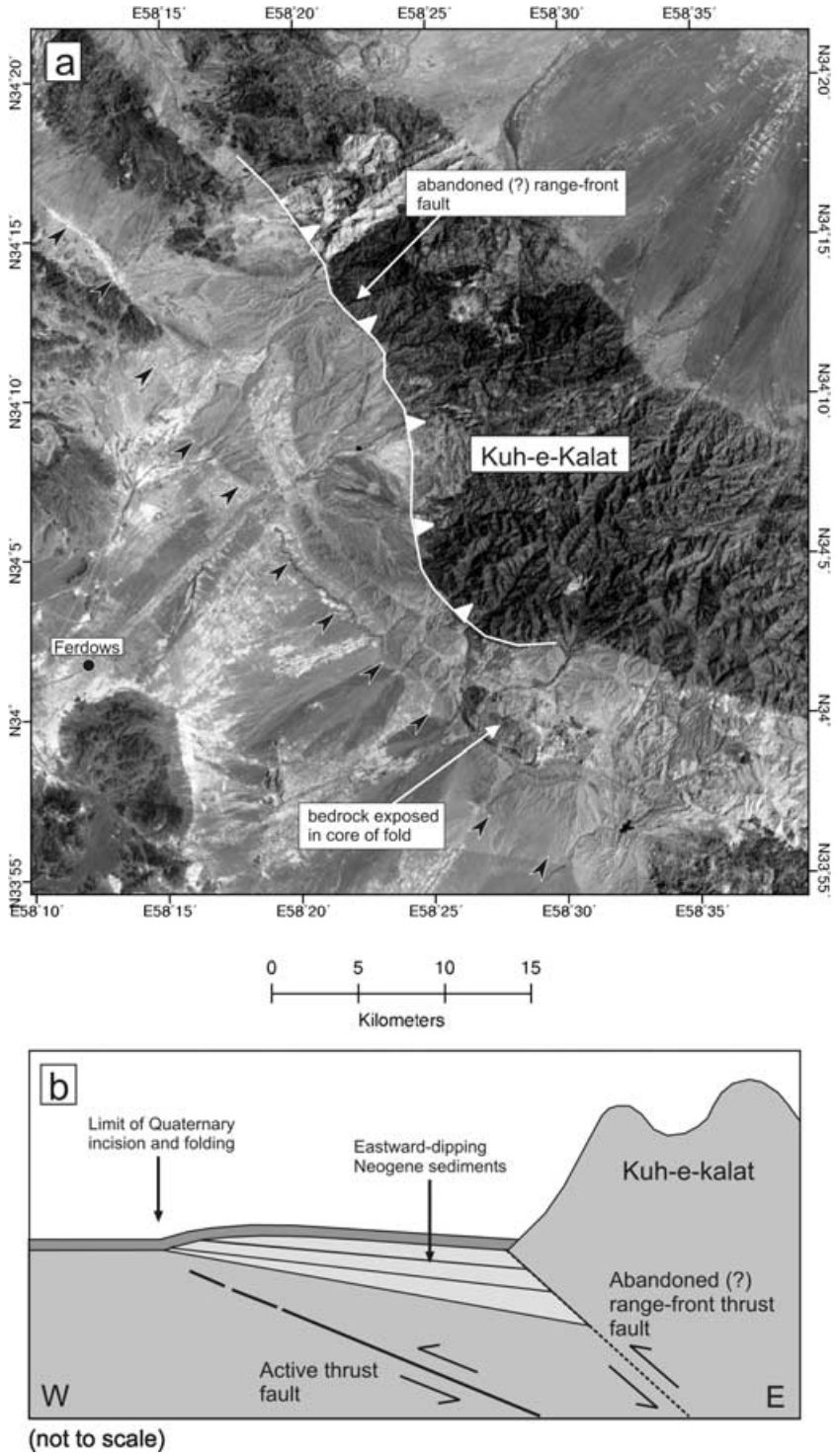

Figure 10. (a) LANDSAT image of folding at Ferdows marked by black arrows (see Fig. 2 for location). Walker *et al.* (2003) relate this to growth above an eastward-dipping thrust fault responsible for the 1968 September 1 and 1968 September 4 earthquakes (see Table 2). (b) Cartoon cross-section through the Ferdows fold and Kuh-e-Kalat. Eastward-dipping Neogene sediments appear to have been deposited in the footwall of a thrust fault along the mountain range-front (the white toothed line in Fig. 10a). Present-day activity has migrated westwards and has caused uplift and folding of Quaternary alluvium and river terraces.

is seen in the central part (Figs 11 and 12c) with a vertical up to the east component. However, unambiguous tectonic drainage offsets are not seen at the resolution of the satellite images.

The 1941 February 16 Muhammadabad earthquake (Table 1) destroyed several settlements and killed 680 people in the sparsely populated region (Ambraseys & Melville 1982, Table 1;). Probable surface ruptures are shown in Figs 11 and 12(c). They were restricted to *ca* 10 km length within a region of bedrock exposure at the northern end of the fault. Weathered *en echelon* cracks, observed in 1978 (Ambraseys & Melville 1982) suggest right-lateral faulting. Local

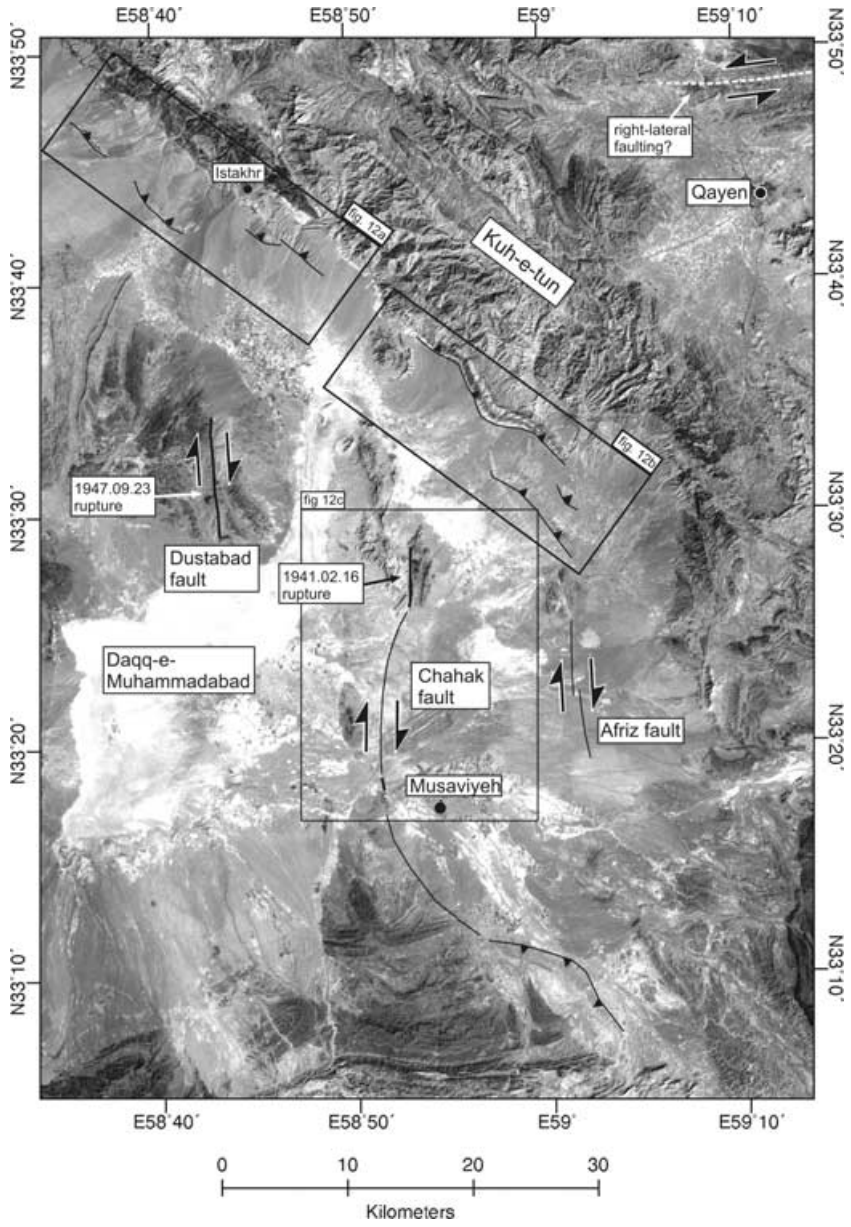

Figure 11. LANDSAT TM+ image of the Muhammadabad fault system SW of Dasht-e-Bayaz (see Fig. 2 for location). Three north–south right-lateral strike-slip faults can be identified. The Dustabad and Chahak faults have ruptured in destructive earthquakes in 1941 and 1947 (represented by thickened black lines; see Table 1). These strike-slip faults appear to end in thrust faults that have reactivated parts of the Kuh-e-Tun range-front. Boxes show the locations of later figures. Possible faulting can be seen in the NE of the image, *ca* 10 km north of Qayen.

people remember initial vertical offsets of *ca* 50 cm downthrown to the west (Ambraseys & Melville 1982).

No surface ruptures have been identified for the 1962 April 1 Musaviyeh earthquake (Table 1). However, the localized damage distribution directly south of the Muhammadabad epicentral region suggests that it also occurred on the Chahak fault (Figs 11 and 12c; Ambraseys & Melville 1982).

At their southern end, the Holocene fault scarps can be traced into a zone of folding south of Musaviyeh (Fig. 11). Although the Chahak fault cannot be traced on satellite imagery north of *ca* 33.5°N to the Kuh-e-Tun range (Fig. 11), a zone of folding is seen *ca* 20 km north of the strike-slip trace (Figs 11 and 12a). It is reasonable to suppose that the Chahak fault extends to the intersection with these folds. The northern part of the Dustabad fault (which apparently ruptured in 1947) and the Afriz fault are also indistinguishable at the resolution of the satellite imagery, but end in zones of folding along the flanks of Kuh-e-Tun (Figs 11 and 12).

4.2.3 The Afriz fault

No historical earthquakes are known for this fault. It appears on aerial photographs as a series of discontinuous scarps that displace drainage right-laterally. However, these features are too small to be seen on LANDSAT TM+ images (Fig. 11), and the only expression of active strike-slip faulting is in the straight edge of cultivated fields, coincident with the fault. However, at its northern end there is clear evidence of active folding splaying northwestwards from the Afriz strike-slip fault (Figs 11 and 12b). Again, the strike-slip fault probably links with a thrust fault at its end. Afriz is surrounded by mountains on three sides and rapid alluvial sedimentation may help

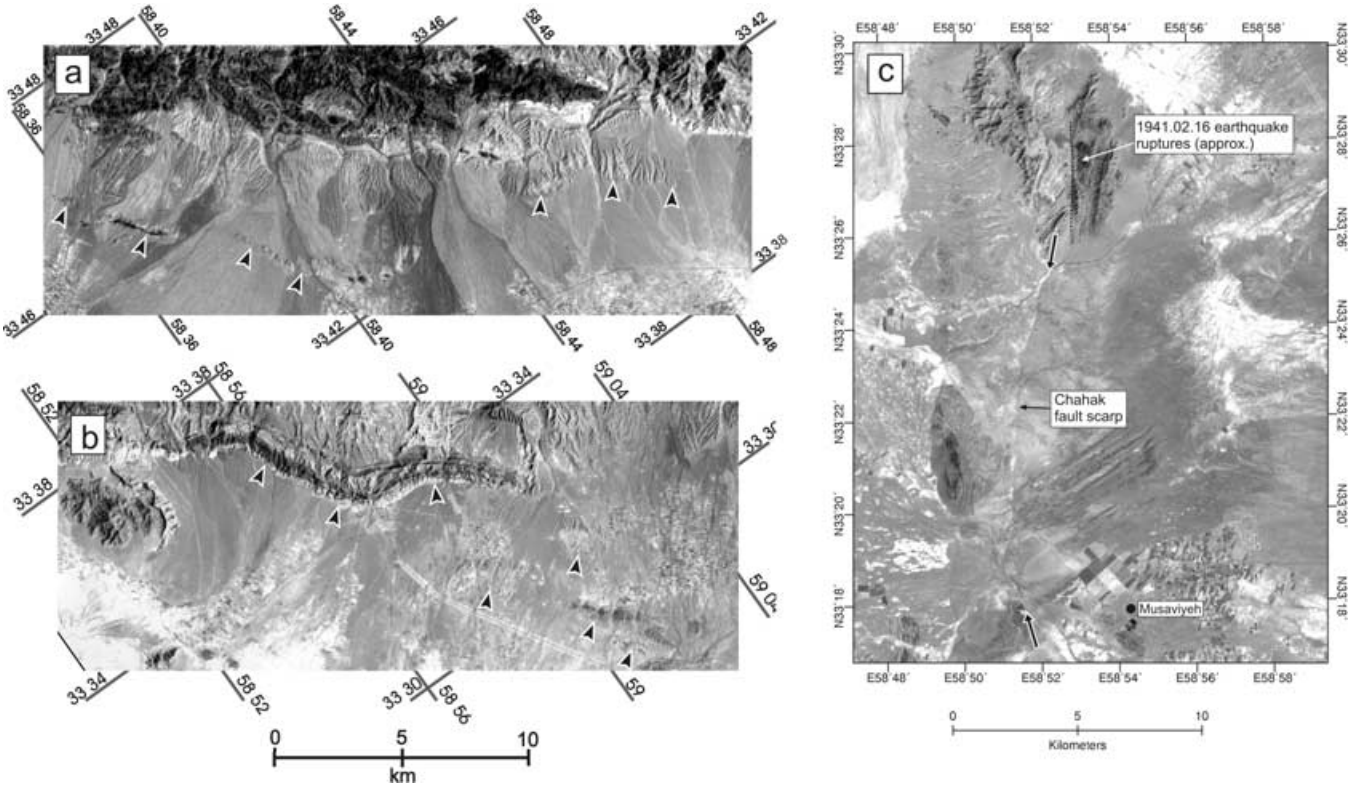

Figure 12. (a) LANDSAT TM+ image of folding along the Kuh-e-Tun range front. Fold fronts are marked with black arrows. See Fig. 11 for location. (b) SE continuation of Fig. 12(a). In both (a) and (b) folding appears to be active in the Quaternary, with uplifted fans and river incision to the north of the range-front. (c) LANDSAT TM+ view of the Chahak cumulative fault scarps. These form a southward continuation of the 1941 February 16 Muhammadabad surface ruptures.

to mask cumulative scarps associated with faulting that are seen elsewhere.

4.2.4 The Muhammadabad fault system: a summary

The right-lateral strike-slip faults of the Muhammadabad system appear to end in the north against the thrusts faults of the Kuh-e-Tun range-front. These right-lateral faults generated destructive earthquakes in 1941, 1947 and 1962 (Table 1; Ambraseys & Melville 1982) and yet are subtle features with probably only small total cumulative offsets. Only one of the faults (the Chahak fault) is easily observed on LANDSAT TM+ imagery, and this is due to its slight vertical component. The other two faults might be unclear because they are in bedrock (the Dustabad fault), or in a region of rapid alluvial sedimentation (the Afriz fault). However, folding at the ends of each of these faults is readily identifiable on satellite imagery, due to the folds being uplifted above the level of fluvial erosion and alluvial sedimentation.

4.3 Gonabad and Qayen: faulting parallel to Dasht-e-Bayaz

Another diffuse zone of faulting is seen at Gonabad, north of the Dasht-e-Bayaz fault (Fig. 13a). Two >20 km long, east–west faults occur in a zone *ca* 20 km wide. The faults cut alluvium. No offset markers are identified. However, the linear east–west trend of the faults suggests that they are strike-slip faults, and their east–west orientation indicates that they are probably left-lateral. Several historical earthquakes are known to have damaged the Gonabad region (Ambraseys & Melville 1982; Berberian & Yeats 1999, Table 1), although these events are not attributed to any individual fault.

It is difficult to see if similar deformation occurs in the Qayen region to the south of the fault. The region is mountainous, and as described earlier, it can be difficult to see faults within such terrain. However, there are indications of surface uplift and incision of alluvial fans in the regions north of Qayen (Figs 2 and 11). Berberian & Yeats (1999) describe E–W faults in this region. Furthermore, teleseismic epicentre locations of the 1976 November 7 and 1979 January 16 earthquakes (Fig. 2 and Table 2) are situated close to Qayen. Even allowing for a 10–15 km uncertainty in location (Berberian 1979; Ambraseys 2001), this indicates that active strike-slip faulting does occur in the region immediately north of Qayen. However, we cannot be sure that the earthquakes indicate left-lateral movement on faults parallel to the Dasht-e-Bayaz fault, rather than right-lateral faulting on north–south faults, as at Muhammadabad.

4.4 East of Dasht-e-Bayaz: the Niazabad fault

The Niazabad fault forms a continuous scarp running eastwards from Niazabad towards the Afghan border (Figs 2 and 13b). Haghipour & Amidi (1980) infer that it joins with the eastern end of the Dasht-e-Bayaz fault through the encrusted salt flats east of Kuh-e-Kheybar (white region at *ca* 34°15′N 60°E on Fig. 2). However, there are no indications on satellite imagery or aerial photographs that a continuous fault crosses this region (Fig. 13b). The westernmost *ca* 15 km of the fault is a simple south-facing scarp trending *ca* 80°. East of 60°20′E, the fault changes strike to *ca* 100° and is accompanied by folding at the surface (Fig. 13b). The fault scarp and folds can be traced to the Afghan border (Fig. 1c), but it is not clear if they extend any further east.

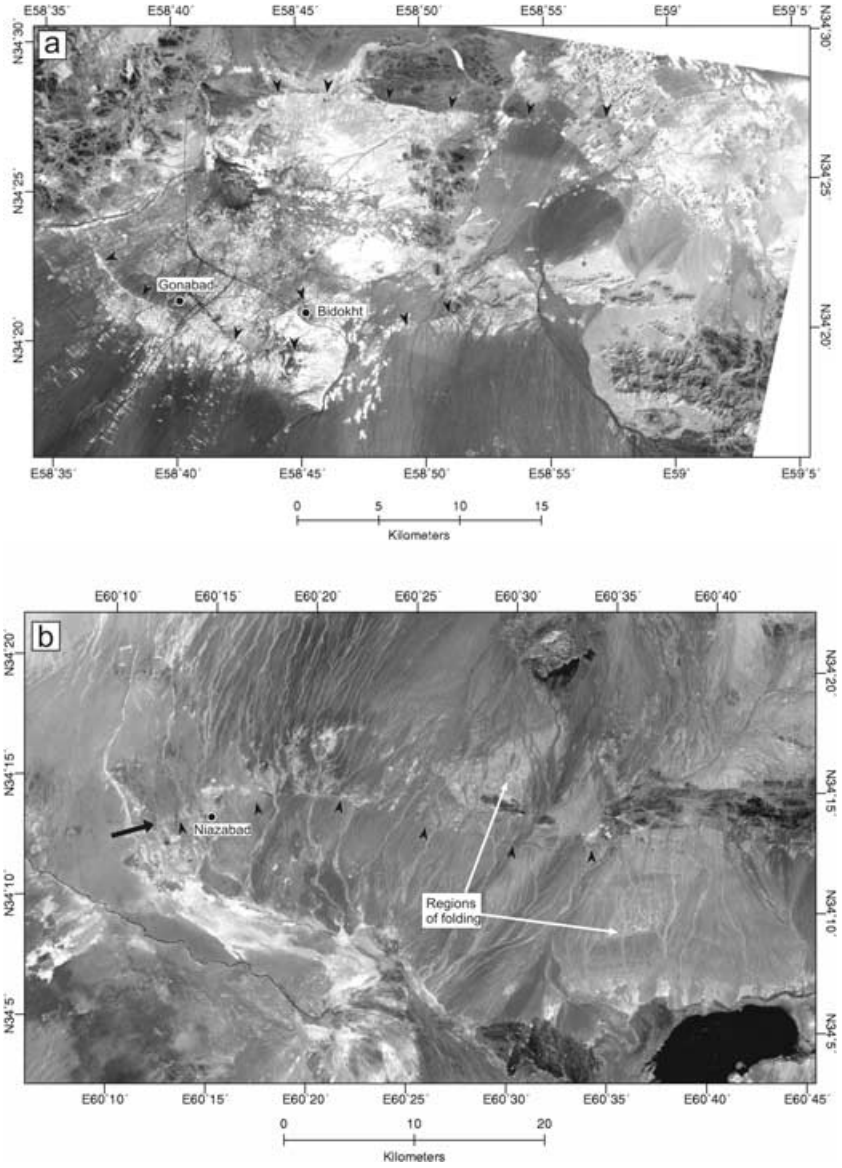

Figure 13. (a) ASTER image of the Gonabad fault system to the north of Dasht-e-Bayaz (see Fig. 2 for location). Two main east–west fault scarps can be seen (marked by black arrows). Several smaller scarps are also present. The faults cause drainage incision on their southern sides. The linear scarps and east–west orientation suggest that they are left-lateral faults. (b) LANDSAT view of the Niazabad fault scarp. This is marked by black arrows. West of longitude 60°12′E, no deformation can be seen. Between longitude 60°12′E and 60°20′E, the fault has a simple south-facing scarp that trends *ca* 80°. East of longitude 60°20′E, the fault changes orientation to *ca* 100° and acquires a greater component of shortening, seen as folding at the surface.

4.5 Distributed faulting around the Dasht-e-Bayaz fault: a summary

The above discussion demonstrates that distributed active faulting is common throughout the Dasht-e-Bayaz region. E–W left-lateral faults, N–S right-lateral faults and NW–SE thrust faults can all be recognized in the geomorphology. Several of these faults have generated destructive earthquakes [e.g. the AD1238 and AD1675 earthquakes at Gonabad (Table 1), the 1941, 1947 and 1962 earthquakes on the Muhammadabad fault system and 1968 September 1st and 4th Ferdows earthquakes], and pose a continuing seismic hazard to local populations.

Several earthquake epicentres are not attributed to faulting identified from geomorphology (e.g. 1976 November 7 and 1979 January 16, see Table 2 and Fig. 2). The Dustabad fault (Fig. 11) is not visible on satellite imagery either, and is only identified due to surface ruptures developed in 1947 (Ambraseys & Melville 1982). It is likely that active faults other than those described here also exist and may cause destructive earthquakes.

5 TECTONIC IMPLICATIONS

If the Dasht-e-Bayaz fault transfers right-lateral shear between central Iran and Afghanistan to the mountains of northern Iran (Jackson & McKenzie 1984; Jackson *et al.* 1995), it must do so by rotating clockwise about a vertical axis (Bayasgalan *et al.* 1999; Berberian *et al.* 2000 ; Figs 14a and b). The major part of the *ca* 20 mm yr^{-1} of right-lateral shear is probably taken up across the faults of the Sistan suture zone, directly to the south of the Dasht-e-Bayaz fault, where bedrock offsets of $\geq$50 km are seen (Tirrul *et al.* 1981; Walker & Jackson 2002). If the Dasht-e-Bayaz fault has accommodated $\geq$50 km of N–S right-lateral shear, it would have rotated clockwise by

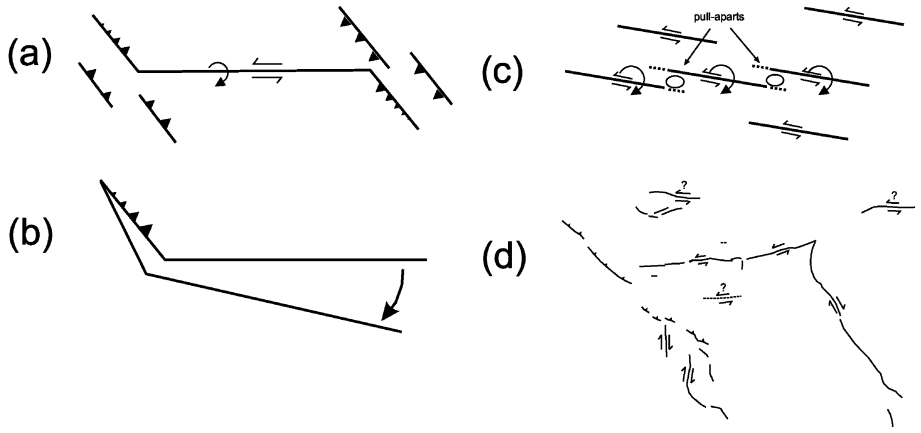

Figure 14. (a) The Dasht-e-Bayaz fault can accumulate displacement and accommodate right-lateral shear by rotating clockwise. This configuration requires that the fault ends in thrust faults that die away from the junction of the two faults, and also allows the rotating strike-slip fault to be associated with other thrust faults that do not need to rotate. Note that this configuration requires internal deformation within the blocks surrounding the fault. This figure is adapted from Berberian *et al.* (2000). (b) If the slip vectors on the thrusts and strike-slip faults are not identical (as is suggested by the Dasht-e-Bayaz and Ferdows earthquake sequences, see Table 2), the rotating blocks cannot be rigid and must deform internally. This figure is adapted from Bayasgalan *et al.* (1999). (c) Several aligned fault segments rotating independently will result in a breaking apart of the fault, creating small pull-aparts between fault segments, and abandoned scarps at the ends of the segments. Feedback between aligned segments will localize strain onto these strands and may eventually cause them to coalesce to produce a new through-going structure. (d) Sketch of observed faulting in the Dasht-e-Bayaz region. It is likely that additional active faults remain unobserved.

at least 15° (and, we might expect, up to twice this amount of rotation, as discussed later). Fig. 9 shows a simple model in which N–S shear is accommodated by clockwise rotation about vertical axes of fault-bounded blocks. This model does not account for the internal deformation that must occur within the blocks, but is a useful way of determining the fault displacements introduced by rotations about vertical axes. The total fault offset caused by rotation in Fig. 9 varies with the width of the rotating blocks, but for a block of *ca* 100 km width, would require ≥25 km of left-lateral displacement. Displacements of this amount are not seen. Total left-lateral displacements across the fault are estimated at 4–5 km, which would account for <20 km of right-lateral N–S shear (Fig. 9). The estimates of total left-lateral offset are from displaced bedrock features and so are a maximum value. The Dasht-e-Bayaz fault must therefore either be relatively unimportant in accommodating right-lateral shear in eastern Iran, or must be a relatively young feature.

If the Dasht-e-Bayaz fault is in an early stage of its development, it provides an important insight into the ways in which strike-slip faults grow and interact. We have shown that diffuse deformation occurs all around the Dasht-e-Bayaz fault: this may be a consequence of rapid rotations about a vertical axis, which would require internal deformation of the blocks to either side of the fault (Fig. 14b). However, as the Dasht-e-Bayaz fault has not accommodated a large amount of clockwise rotation, it is not likely to have caused the widespread distributed faulting that is seen. The left-stepping, segmented nature of the fault suggest to us that the Dasht-e-Bayaz fault may not be a through-going structure at all, but instead composed of several small aligned faults (Fig. 14c), which may eventually coalesce into a single, through-going fault. A localization of strain onto a few aligned fault strands that eventually coalesce has already been suggested as a mechanism for normal fault migration, both theoretically (Cowie 1998) and based on field evidence (Goldsworthy & Jackson 2000, 2001).

The Doruneh fault (Fig. 1c) changes in strike by 40–50° near longitude *ca* 58°E. West of this point its orientation is WSW–ENE. East of this point, the fault swings round to an ESE–WNW orientation, becoming perpendicular to the direction of regional shortening (Fig. 1b). The prominent bend in the Doruneh fault is north of the active faults of the Sistan suture zone (Fig. 1c), where we expect large amounts of the *ca* 20 mm yr^{-1} of Iran–Afghanistan right-lateral shear to be taken up, and hence clockwise fault rotations of up to 6° per Myr. If the Doruneh fault has been active since *ca* 5 Ma, when we believe the present-day tectonic configuration initiated, this would account for up to 30° of clockwise rotation, which goes some way towards explaining the prominent bend near longitude 58°E. It therefore appears that the Doruneh fault could have accommodated upwards of 50 km of right-lateral shear. The right-lateral fault systems on the western margin of the Dasht-e-Lut (the Nayband and Kuh-Banan faults) are still active, but with slip-rates of *ca* 2 mm yr^{-1}, which is much slower than those east of the Dasht-e-Lut (Walker & Jackson 2002).

We conclude that the left-lateral slip and clockwise rotation of the Dasht-e-Bayaz fault has not accommodated a large amount of the expected *ca* 50 km of N–S right-lateral shear between central Iran and Afghanistan and may be a relatively young structure. The Dasht-e-Bayaz fault occurs only across the region east of longitude 58°E, where the Doruneh fault system becomes perpendicular to the NNE–SSW regional convergence and shows Holocene and historical (the 1336AD Khwaf earthquake; Ambraseys & Melville 1982) thrust faulting on the Jangal faults (Fig. 1c). This eastern part of the Doruneh fault can no longer rotate away from the direction of regional shortening. This situation may have favoured the initiation of a new strike-slip fault across this region. The Doruneh fault east of longitude 58°E and the Dasht-e-Bayaz fault are expressed very differently, with distinct orientations. The Doruneh fault shows a large shortening component in the form of thrust faulting, and there is topographic relief across the Doruneh fault of *ca* 1 km, in contrast to the subdued relief across the Dasht-e-Bayaz fault (e.g. Fig. 2). West of longitude 58°E, the Doruneh fault is still able to rotate clockwise and accommodate right-lateral shear, and so no new fault has initiated here.

6 CONCLUSIONS

We conclude that the onset of faulting at Dasht-e-Bayaz is relatively recent, probably post-dating earlier and more substantial offset on

the Doruneh fault. There are indications both in the seismicity and the geomorphology that a new, through-going fault is emerging at Dasht-e-Bayaz due to the linking of several aligned fault segments. These aligned segments are part of a larger distributed population including faults at Gonabad, Muhammadabad and Niazabad. Our conclusion is that these strike-slip fault systems change with time, by rotation about vertical axes and by the initiation of new through-going faults. This result has importance for the development of strike-slip fault zones, which are developed worldwide in many regions of both continental shortening and extension.

This study also highlights the importance of combining information about the nature of the faulting at depth from seismology, and the long-term development of the faulting recorded in the geomorphology to gain a better understanding of the ways in which the faulting evolves and is expressed at the surface. Modern satellite imagery enhances our ability to observe subtle geomorphic indicators of active faulting on a regional scale, and aids the study of active tectonics and estimates of seismic hazard to local populations.

ACKNOWLEDGMENTS

The authors would like to thank M. T. Khorehei and M. Qorashi of the Geological Survey of Iran in Tehran for their continued support of this work and for enabling us to visit the Ferdows region in several field seasons. N. N. Ambraseys kindly provided original maps of the 1968 earthquake ruptures and allowed reprinting of several aerial photographs. Helpful comments and reviews were provided by R. Bilham, P. England and D. McKenzie. RW was supported by a NERC studentship. This work was supported by the NERC Centre for the Observation and Modelling of Earthquakes and Tectonics (COMET), and forms Cambridge Earth Science Contribution No. 7278.

REFERENCES

Alavi-Naini, M., 1983. *Geological quadrangle map of Iran No. K6 (Gonabad sheet), scale 1:250,000*, Geological Survey of Iran

Ambraseys, N.N., 2001. Reassessment of earthquakes, 1900–1999, in the Eastern Mediterranean and the Middle East, *Geophys. J. Int.*, **145**, 471–485.

Ambraseys, N.N. & Tchalenko, J.S., 1969. The Dasht-e-Bayas (Iran) earthquake of August 31, 1968: A field report, *Bull. seism. Soc. Am.*, **59**, 1751–1792.

Ambraseys, N.N. & Melville, C.P., 1982. *A History of Persian Earthquakes*, Cambridge University Press, UK.

Baker, C., 1993. Active Seismicity and Tectonics of Iran, PhD thesis (unpublished), University of Cambridge, UK.

Bayasgalan, A., Jackson, J., Ritz, J-F. & Carretier, S., 1999. Field examples of strike-slip fault terminations in Mongolia and their tectonic significance, *Tectonics*, **18**, 394–411.

Berberian, M., 1976. *Contribution to the seismotectonics of Iran (Part II)*, Report No. 39, Geological Survey of Iran.

Berberian, M., 1979. Evaluation of instrumental and relocated epicentres of Iranian earthquakes, *Geophys. J. R. astr. Soc.*, **58**, 625–630.

Berberian, M. & Yeats, R.S., 1999. Patterns of Historical Earthquake Rupture in the Iranian Plateau, *Bull. seism. Soc. Am.*, **89**, 120–139.

Berberian, M. & Yeats, R.S., 2001. Contribution of archaeological data to studies of earthquake history in the Iranian Plateau, *J. Struct. Geol.*, **23**, 563–584.

Berberian, M., Jackson, J.A., Qorashi, M., Khatib, M.M., Priestley, K., Talebian, M. & Ghafuri-Ashtiani, M., 1999. The 1997 May 10 Zirkuh (Qa'enat) earthquake (M_w 7.2): faulting along the Sistan suture zone of eastern Iran, *Geophys. J. Int.*, **136**, 671–694.

Berberian, M., Jackson, J.A., Qorashi, M., Talebian, M., Khatib, M.M. & Priestley, K., 2000. The 1994 Sefidabeh earthquakes in eastern Iran: blind thrusting and bedding-plane slip on a growing anticline, and active tectonics of the Sistan suture zone, *Geophys. J. Int.*, **142**, 283–299.

Behzadi, H., 1976. The tectonic history of east-central Iran, *PhD thesis*, University of Leeds, UK.

Chu, D. & Gordon, R.G., 1998. Current plate motions across the Red Sea, *Geophys. J. Int.*, **135**, 313–328.

Cowie, P.A., 1998. A healing-reloading feedback control on the growth rate of seismogenic faults, *J. Struct. Geol.*, **20**, 1075–1087.

DeMets, C., Gordon, R.G., Argus, D.F. & Stein, S., 1994. Effect of recent revisions to the geomagnetic reversal time scale on estimates of current plate motions, *Geophys. Res. Lett.*, **21**, 2191–2194.

Devlin, W.J., Cogswell, J.M., Gaskins, G.M., Isaksen, G.H., Pitcher, D.M., Puls, D.P., Stanley, K.O. & Wall, G.R.T., 1999. South Caspian basin: young, cool, and full of promise., *GSA today*, **9**, 1–9.

England, P. & Molnar, P., 1990. Right-lateral shear and rotation as the explanation for strike-slip faulting in eastern Tibet, *Nature*, **344**, 140–142.

Engdahl, E.R., van der Hilst, R. & Buland, R., 1998. Global teleseismic earthquake relocation with improved travel times and procedures for depth determination, *Bull. seism. Soc. Am.*, **88**, 722–743.

Falcon, N.L., 1974. Southern Iran: Zagros mountains, *Geol. Soc. Lond. Spec. Pub.*, **4**, 199–211.

Goldsworthy, M. & Jackson, J., 2000. Active normal fault evolution in Greece revealed by geomorphology and drainage patterns, *J. geol. Soc. Lond.*, **157**, 967–981.

Goldsworthy, M. & Jackson, J., 2001. Migration of activity within normal fault systems: examples from the Quaternary of mainland Greece, *J. Struct. Geol.*, **23**, 489–506.

Haghipour, A. & Amidi, M., 1980. The November 14 to December 25, 1979 Ghaenat earthquakes of northest Iran and their tectonic implications, *Bull. seism. Soc. Am.*, **70**, 1751–1757.

Hessami, K., 2002. Tectonic History and Present-Day Deformation in the Zagros Fold-Thrust Belt, PhD thesis, University of Uppsala, Sweden

Holt, W.E., Ni, J.F., Wallace, T.C. & Haines, A.J., 1991. The active tectonics of the Eastern Himalayan Syntaxis and surrounding regions, *J. geophys. Res.*, **96**, 14 595–14 632.

Jackson, J., 2001. Living with earthquakes: know your faults, *J. Earthquake Engineering*, **5**, Special Issue 1, 5–123.

Jackson, J. & McKenzie, D., 1984. Active tectonics of the Alpine-Himalayan Belt between western Turkey and Pakistan, *Geophys. J. R. astr. Soc.*, **77**, 185–264.

Jackson, J., Haines, J. & Holt, W., 1995. The accommodation of Arabia-Eurasia plate convergence in Iran, *J. geophys. Res.*, **100**, 15 205–15 219.

Jackson, J., Norris, R. & Youngson, J., 1996. The structural evolution of active fault and fold systems in central Otago, New Zealand: evidence revealed by drainage patterns, *J. Struct. Geol.*, **18**, 217–234.

Jackson, J., Priestley, K., Allen, M. & Berberian, M., 2002. Active tectonics of the South Caspian basin, *Geophys. J. Int.*, **148**, 214–245.

Jestin, F., Huchon, P. & Gaulier, J.M., 1994. The Somalia plate and the East African Rift System: present-day kinematics, *Geophys. J. Int.*, **116**, 637–654.

Keller, E.A., Zepeda, R.L., Rockwell, T.K., Ku, T.L. & Dinklage, W.S., 1998. Active tectonics at Wheeler Ridge, southern San Joaquin Valley, California, *Geological Society of America Bulletin*, **110**, 298–310.

Kurushin, R.A., Bayasgalan, A., Olziybat, M., Enhtuvshin, B., Molnar, P., Bayarsayhan, Ch., Hudnut, K.W. & Lin, J., 1997. The surface rupture of the 1957 Gobi-Altay, Mongolia, earthquake, *Geol. Soc. Am. Spec. Paper*, p. 320.

Lasserre, C. et al, 1999. Postglacial left slip rate and past occurrence of $M > 8$ earthquakes on the western Haiyuan fault, Gansu, China, *J. geophys. Res.*, **104**, 17 633–17 651.

McCaffrey, R. & Abers, G., 1988. *SYN3: a program for inversion of teleseismic body waveforms on microcomputers*,, Hanscomb Air Force Base, MA.

McCaffrey, R., Zwick, P. & Abers, G., 1991. SYN4 Program, *IASPEI Software Library*, **3**, 81–166.

McKenzie, D., 1972. Active tectonics of the Mediterranean region, *Geophys. J. R. astr. Soc.*, **30**, 109–185.

Mehryar, M. & Kabiri, A., 1986. *Preliminary report on the Delazian (Cheshmeh Shaikh) archaeological site, Asar, Sazeman Meli Hefazat Asar Bastani Iran*, **Vols 12–14** 3–46, Esfand, Tehran (in Persian).

Meyer, B., Tapponnier, P., Bourjot, L., Metivier, F., Gaudemar, Y., Peltzer, G., Shunmin, G. & Zhitai, C., 1998. Crustal thickening in Gansu-Qinghai, lithospheric mantle subduction, and oblique, strike-slip controlled growth of the Tibet plateau, *Geophys. J. Int.*, **135**, 1–47.

Molnar, P. & Deng, Q., 1984. Faulting associated with large earthquakes and the average rate of deformation in central and eastern Asia, *J. geophys. Res.*, **89**, 6203–6227.

Molnar, P. & Tapponnier, P., 1975. Cenozoic tectonics of Asia: Effects of a continental collision, *Science*, **189**, 419–426.

Nabelek, J., 1984. Determination of earthquake source parameters from inversion of body waves, PhD thesis, MIT, MA, USA.

Replumaz, A., Lacassin, R., Tapponnier, P. & Leloup, P.H., 2001. Large river offsets and Plio-Quaternary dextral slip rate on the Red River fault (Yunnan, China), *J. geophys. Res.*, **106**, 819–836.

Sella, G.F., Dixon, T.H. & Mao, A., 2002. REVEL: A model for recent plate velocities from space geodesy, *J. geophys. Res.*, **107**, 10.1029/2000JB000033.

Talebian, M. & Jackson, J., 2002. Offset on the Main Recent Fault of NW Iran and implications for the late Cenozoic tectonics of the Arabia-Eurasia collision zone, *Geophys. J. Int.*, **150**, 422–439.

Tatar, M., Hatzfeld, D., Martinod, J., Walpersdorf, A., Ghafori-Ashtiany, M. & Chery, J., 2002. The present-day deformation of the central Zagros from GPS measurements, *Geophys. Res. Lett.*, **29**, 1927–1930.

Taymaz, T., Jackson, J. & McKenzie, D., 1991. Active tectonics of the north and central Aegean Sea, *Geophys. J. Int.*, **106**, 433–490.

Tchalenko, J.S. & Ambraseys, N.N., 1970. Structural analysis of the Dasht-e-Bayaz (Iran) earthquake fractures, *Geol. Soc. Am. Bull.*, **81**, 41–60.

Tchalenko, J.S. & Ambraseys, N.N., 1973. Earthquake destruction of adobe villages in Iran, *Annali di Geofisica*, **26**, 357–389.

Tchalenko, J.S. & Berberian, M., 1975. Dasht-e-Bayaz fault, Iran: Earthquake and earlier related structures in ck, *Geol. Soc. Am. Bull.*, **86**, 703–709.

Tirrul, R., Bell, I.R., Griffis, R.J. & Camp, V.E., 1983. The Sistan suture zone of eastern Iran, *Geol. Soc. Am. Bull.*, **94**, 134–150.

Walker, R. & Jackson, J., 2002. Offset and evolution of the Gowk fault, S.E. Iran: a major intra-continental strike-slip system, *J. Struct. Geol.*, **24**, 1677–1698.

Walker, R., Jackson, J. & Baker, C., 2003. Surface expression of thrust faulting in eastern Iran: source parameters and surface deformation of the 1978 Tabas and 1968 Ferdows earthquake sequences, *Geophys. J. Int.*, **152**, 749–765.

Zwick, P., McCaffrey, R. & Abers, G., 1995. MT5 Program, *IASPEI Software Library*, **4**.